ChemistrySelect
Chemistry Europe
European Chemical Societies Publishing

RESEARCH ARTICLE OPEN ACCESS

Synthesis and Characterization of Glyco-Decorated Silsesquioxane-Metallosalen Complexes

Hanni Haapsaari | Tytti Taipale | Petri Tähtinen | Anssi Peuronen | Pasi Virta

Department of Chemistry, University of Turku, Turku, Finland

Correspondence: Pasi Virta (pamavi@utu.fi)

Received: 22 January 2026 | **Accepted:** 26 January 2026

Keywords: artificial nucleases | glycoclusters | metallosalens | organometal complexes | silsesquioxanes

ABSTRACT

Cube-octameric silsesquioxanes (COSS) present interesting opportunities in several applications due to their rigid inorganic and biocompatible silicate core combined with tunable, well-oriented corner functionalities. In the present study, multivalent mannose-decorated COSS-metallosalen complexes, as models combining potential catalytic activity and cell-targeting moieties in a single structure, were synthesized. The complexes proved to be hydrolytically stable, and their assembly was efficient between a slight excess of salicylaldehyde-derived mannose and an aminopropyl-modified COSS core, followed by complexation with metal ions. The complexes can adopt a D_{4h} or an S_4 geometry with zinc and copper ions, respectively, which affects the orientation of the mannose substituents and the availability of the catalytic metallosalen centers on the COSS core. Potential but modest ribonuclease activity of the complexes was observed. The hydrolytic stability and the efficient assembly of these well-organized complexes can be utilized for the synthesis of other glyco or biomolecule analogues.

1 | Introduction

Nanoparticles and other nanomaterials with custom-made functionalities have become increasingly more attractive in the field of drug development [1]. Among silicananoparticles are cage-like silsesquioxanes, fully condensed polyhedral organosilicon materials with a general formula of $(RSiO_{1.5})_n$, and a diameter of around 1–3 nm [2–5]. They consist of an inorganic silicate core (Si–O–Si) and an exterior organic shell. There can be a different number of silicon atoms in the cage, and trifunctional siloxane cages usually include T6, T8, T10, and T12 structures, of which the highly symmetrical T8 structure $(RSiO_{1.5})_8$ is the most widely studied. In cube-octameric silsesquioxanes (COSS), the fourth position of a silicon atom is bonded with other functional groups, enabling a spherical deployment of eight ligands. Many interesting properties arise from the rigid inorganic core structure: tiny size, good pH tolerance, high mechanical strength, enhanced thermal and chemical stability, good charge transferability, reduced heat transfer coefficient, optical transparency, and resistance to fire. The aforementioned properties have been examined in various applications, including thermal and biomedical (drug delivery, tissue engineering) applications, catalysis, sensors, and energy storage [2–7]. COSS structures are particularly appealing in biomedical applications due to their low toxicity and high biocompatibility, as their hydrolytic degradation leads to well-known primary silsesquioxanes [8, 9]. Cube-shaped T8 COSS structures are highly tailorable in functionality because pendant functionalities allow, for example, the conjugation of different biomolecules such as peptides and carbohydrates [10].

Multivalency improves the specificity and affinity of ligand–receptor interactions as multiple molecular recognition processes occur simultaneously [11–13]. Many biological systems utilize multivalency, for example, in signal transduction, biological recognition processes, and self-organization of matter. Interest has been drawn to the precise assembly of multiple ligands

around a suitable scaffold or nanoparticle, aiming to maximize biological effects [14]. An example of multivalent interactions in biological systems is the reversible binding between lectin receptors and carbohydrates [12, 13]. This interaction is present in several important biological functions like cell–cell and cell–pathogen recognition, immune regulation, and cell-growth regulation. One important lectin–carbohydrate interaction is between mannose receptors on the surfaces of macrophages [12]. Macrophages are part of homeostasis [15–17] and the innate immune system [18–20], however, they have also been shown to be involved in numerous diseases, among them cancer and autoimmune diseases [15, 21, 22]. For example, tumor-associated macrophages (TAMs), where the expression of the mannose receptor (CD206/MRC1) is upregulated [23–25], contribute to tumor growth, angiogenesis, metastasis, immunosuppression, and relapse [26–33]. Therefore, macrophages and their mannose receptors can be important therapeutic targets.

Multivalent systems can also entail several catalytically active functional groups [34]. They can result in the cooperation of the reactive functions and allow multiple catalytic events to take place simultaneously [35]. Lately, nano-catalysis has been explored as an alternative to conventional catalysis since nanoparticles can offer higher stability, dispersibility, activity, and biocompatibility [36]. In recent years, a lot of COSS-based systems have been developed for catalysis [5], including one utilizing metal-coordinating salen ligands [37]. A salen ligand is a tetradentate bis-Schiff base ligand where two equivalents of salicylaldehyde are combined with a diamine. The cooperative effects of multiple metal sites in salen complexes have been shown to be important in several catalytic reactions [38, 39].

Coordination compounds can provide benefits for pharmaceutical applications that may not be achievable with organic compounds [40]. For example, many metal compounds have been used in cancer treatment since they destroy cancer cells by damaging DNA [41]. In nature, the cleavage of nucleic acids is achieved with nucleases [42], enzymes that catalyze the hydrolysis of DNA and RNA, and their catalytic centers usually contain one or two metal ions [43, 44]. Some properties of natural enzymes have been utilized to create artificial nucleases and nanozymes, which aim to mimic a natural catalytic site within an enzyme by combining appropriate functions [35, 45–50].

Here we describe the synthesis and characterization of multivalent COSS-metallosalen-glyco complexes (Scheme 1). 3-azidomethyl-5-*tert*-butyl-salicylaldehyde (**4**), which can be conjugated to any carbohydrate ligand using robust Cu(I)-catalyzed click reaction, was synthesized and condensed with the aminopropyl-modified COSS. The Schiff bases formed were then exposed to divalent metal ions (Zn^{2+} and Cu^{2+}) to obtain the COSS-metallosalen-glyco complexes. Mannose was attached to the complexes, representing a multivalent glyco sphere potential for cell-specific recognition. Crystal structures of the corresponding COSS-di-*tert*-butyl-salen Zn^{2+} and Cu^{2+} complexes show D_{4h} and S_4 geometries, respectively. The variable geometry, depending on the metal ion, contributes to the potential catalytic pockets and the orientation of the glyco substituents on the COSS core. Potential ribonuclease activity of the complexes was also explored.

2 | Results and Discussion

2.1 | Syntheses

3-azidomethyl-5-*tert*-butyl-salicylaldehyde (**4**) was synthesized from 4-*tert*-butylphenol (**1**) via a three-step method (Scheme 1). First, formylation of 4-*tert*-butylphenol with $MgCl_2$/HCHO afforded 5-*tert*-butylsalicylaldehyde (**2**) in 48% yield. Then, halomethylation at C3 of 5-*tert*-butylsalicylaldehyde resulted in 3-bromomethyl-5-*tert*-butylsalicylaldehyde (**3**) in 90% yield. Finally, the benzylic azide was prepared from the salicylaldehyde via nucleophilic displacement at the benzylic bromide moiety using NaN_3 in DMSO, the yield being 97%. Butynyl-mannose **6** was prepared by glycosidation reaction of peracetylated mannose **5** in the presence of $BF_3 \cdot Et_2O$ with a yield of 32%. The salicylaldehyde **4** and the acetylated butynyl-mannose **6** were exposed to copper(I)-catalyzed click reaction (CuAAc), resulting in the salicylaldehyde-mannose compound **7** in 72% yield. The acetylated salicylaldehyde-mannose **7** was deprotected with K_2CO_3 in methanol, yielding 72% salicylaldehyde-mannose **8**.

The aminopropyl-functionalized COSS (**9**) was prepared by hydrolytic condensation of 3-aminopropyltriethoxysilane (APTES) [55], and recrystallization from methanol afforded the product in 13% yield. Finally, the COSS-salen-mannose **10** was synthesized by quantitative condensation between the salicylaldehyde **8** and **9** in the presence of triethylamine in methanol. Product **10** thus contained a COSS-core, four metal-coordinating salen moieties, and an outer layer of mannose carbohydrates, which offered some water-solubility and potential cell surface recognition.

Schiff bases can coordinate metal ions via the imine nitrogen and another group, usually linked to the aldehyde. Metal complexes

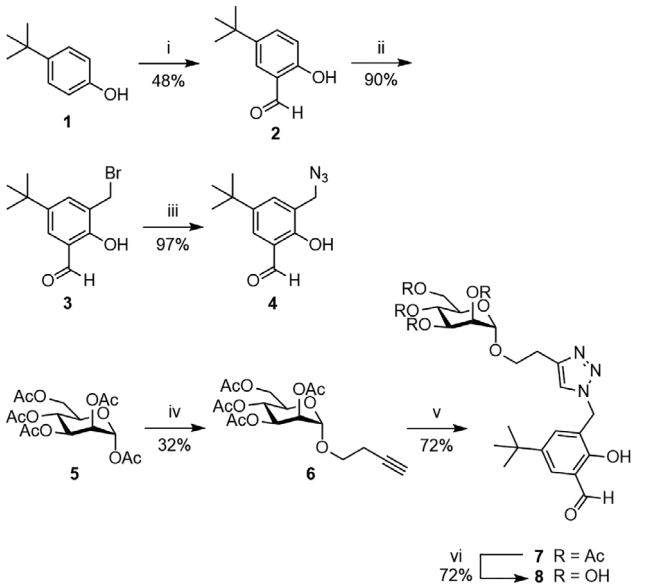

SCHEME 1 | Synthesis of salicylaldehyde-mannose derivative **8**. Conditions: i) paraformaldehyde, $MgCl_2$, Et_3N, MeCN, 24 h, 100°C [51]; ii) paraformaldehyde, HBr, H_2SO_4 (cat.), H_2O, 24 h, 70°C [52]; iii) NaN_3, DMSO, 24 h, r.t. [53]; iv) $BF_3{\cdot}Et_2O$, but-3-yn-1-ol, DCM, 24 h, r.t. [54]; v) $CuSO_4$ (cat.), sodium ascorbate, MeCN/H_2O (1:1 *v/v*), 7 h, r.t.; vi) K_2CO_3, MeOH, 24 h, r.t.

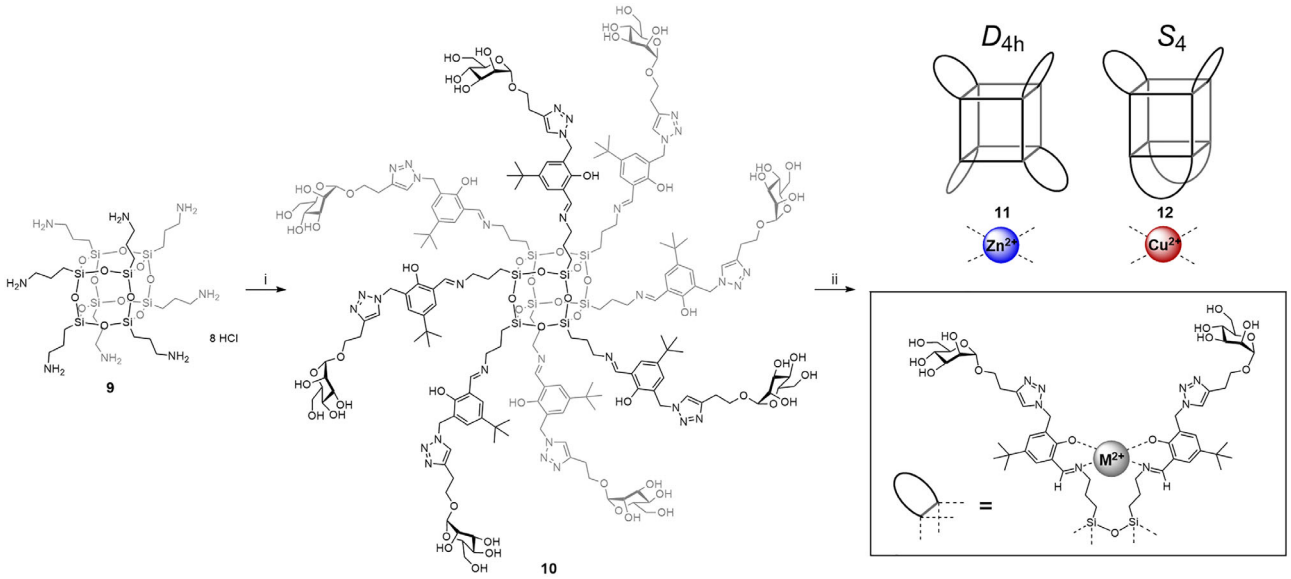

SCHEME 2 | Synthesis of metal complexes of COSS-salen-mannose. Conditions: i) $Zn(OAc)_2 \cdot 2H_2O$, MeOH, 2 h, r.t.; ii) $Cu(OAc)_2$, MeOH, 2 h, r.t.

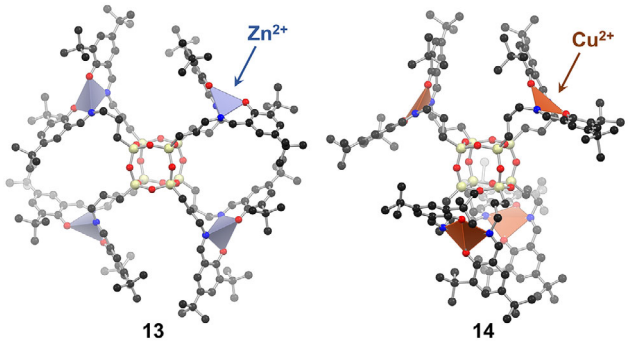

FIGURE 1 | Crystal structures of COSS-di-*tert*-butyl-salen Zn_4 and Cu_4 complexes, representing D_{4h} and S_4 symmetries, respectively.

(**11** and **12**) were obtained by exposing **10** to $Zn(OAc)_2$ or $Cu(OAc)_2$ in anhydrous methanol. The metal complex solutions were divided into 60 nmol aliquots and lyophilized for later use. The authenticity of the complexes **11** and **12** was verified by mass spectroscopy (ESI-TOF) (Figure S23 and S24).

2.2 | Potential Geometry of the COSS-Salen Metal Complexes

COSS-salen **10** incorporates tetradentate N_2O_2 binding sites for four distinct metal ions. Furthermore, the core provides conformational flexibility that can result in two different complex geometries with approximately D_{4h} and S_4 symmetries. These affect the orientation of the sugar moieties and the availability of the metal centers in potential catalytic cavities on the COSS core (Scheme 2). A D_{4h} symmetric complex has previously been authenticated by single-crystal X-ray diffraction studies of a COSS-salen-Zn_4 complex (**13**, Figure 1) [37]. We failed to obtain good-quality and sufficiently stable crystals of **11** and **12** for single-crystal X-ray diffraction studies and, therefore, used complexes **13** and **14** (Figure 1) as analogous model compounds to experimentally confirm the variable D_{4h}/S_4 symmetry in COSS-salen-metal complexes. **13** and **14** were prepared by exposing the synthesized COSS-3,5-di-*tert*-butyl-salen to $Zn(OAc)_2$ and $Cu(OAc)_2$, respectively, in a mixture of chloroform and methanol. In a few days, crystals of **13** and **14** formed in these solutions were collected, and their crystal structures were determined using single-crystal X-ray diffraction. The crystal structure of **13** corresponds to its previously reported structure (CSD-XAGGUL) [56] and shows four Zn^{2+} cations coordinated to the chelating groups in a distorted tetrahedral fashion (d_{Zn-O} = 1.91–1.92 Å and d_{Zn-N} = 1.98–2.02 Å). As discussed above, and previously by Janeta et al. [37], **13** adopts a D_{4h} symmetric geometry, resulting in four approximately equally sized molecule binding pockets, each situated between two of the metal bearing groups. These cavities are large enough to encapsulate one chloroform molecule each, and due to their proximity to the metals, they may serve a significant role in catalytic processes involving the metal centers. The crystal structure of the Cu^{2+} complex (**14**) is similarly a chloroform solvate with a ca. 25% larger unit cell volume compared to **13**, suggesting a significantly higher solvent content in the crystals (see refinement details in SI, Table S1). In contrast to **13**, **14** displays an S_4 symmetric structure due to the different sequence in which the coordinating groups are connected to the Cu^{2+} centers (bond lengths: d_{Cu-O} = 1.89–1.92 Å and d_{Cu-N} = 1.96–1.97 Å; Figure 1). This can be addressed to the noticeably more flattened coordination environment of the Cu^{2+} ions, with a geometry index of τ_4 = 0.29–0.33 [57], compared to Zn^{2+} with τ_4 = 0.74–0.75 (where τ_4 = 1 corresponds to ideal tetrahedral coordination), causing less intramolecular steric strain between the *tert*-butyl groups in the S_4 symmetric configuration. In this geometry, **14** contains only two distinct cavities with one chloroform molecule included in each (Figure S25). Based on this crystallographic evidence, i.e., the metal coordination-driven selection between the D_{4h} and S_4 symmetries in **13** and **14**, it is likely that respective geometries are displayed by the Zn^{2+} and Cu^{2+} metal complexes of COSS-salen-mannose, **11**, and **12**, with the same tetranuclear core moiety. For **11** and **12**, this would mean that the mannose groups have different orientations in these two complexes, which can affect their catalytic perfor-

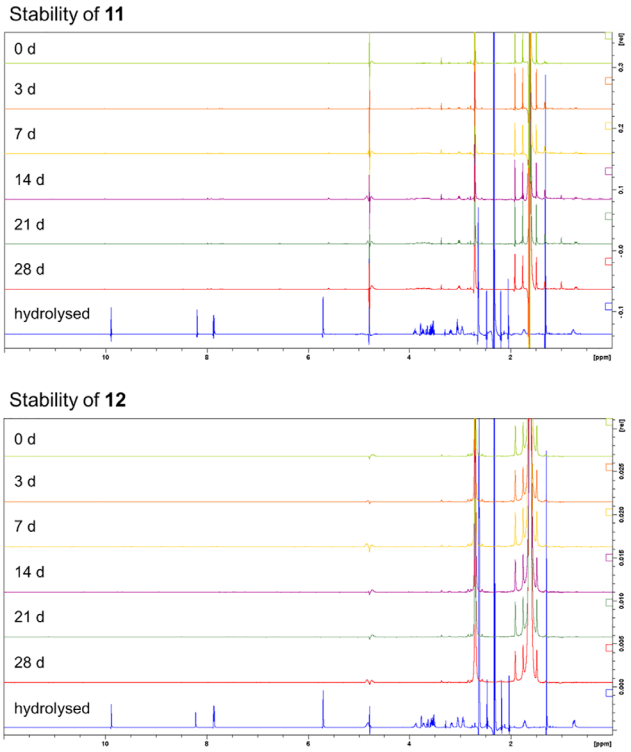

FIGURE 2 | ^{1}H NMR analyses of the stabilities of the metal complexes. 200 μM **11**/**12** in a 3:1 (*v*/*v*) mixture of cacodylate buffer (0.1 M in D_2O, pH 7.5) and DMSO-*d6*. A change in pH due to the addition of 5 μL concentrated H_2SO_4 shifts the signal positions slightly.

mances and potential binding properties. However, the aqueous environment and the substituent effect in **11** and **12** can change the energetically most favored geometry of the complexes.

2.3 | Hydrolytic Stability of the Metal Complexes

Metallosalens are shown to be relatively stable hydrolytically [39, 58]. Coordination of metal ions stabilizes the complexes and prevents hydrolysis of the corresponding imines. To evaluate the stability of the complexes **11** and **12**, they were incubated in hydrolytic conditions, and the potential hydrolysis was monitored by NMR (Figure 2). The experiments were carried out in a 3:1 (*v*/*v*) mixture of cacodylate buffer (0.1 M in D_2O, pH 7.5) and DMSO-*d6*. ^{1}H NMR spectra were recorded as soon as possible after dissolving and after 3, 7, 14, 21, and 28 days. A reference monitoring was performed with compound **10** without any metals (Figure S26). As the compound degrades, the signals from the hydrolysis products (i.e., no metal coordinated) are clear and distinct, and the aldehyde proton at around 10 ppm is distinguishable. To demonstrate this, ^{1}H NMR spectra were recorded in identical conditions but with the addition of 5 μL concentrated sulfuric acid to the NMR samples to purposefully hydrolyze the complexes (the spectra at the bottom, Figure 2). Consequently, the appearance of distinct signals, and especially the signal from the aldehyde proton, indicates hydrolytic degradation of the coordination compounds. In the stability tests, the lack of distinct signals therefore indicates no significant hydrolytic degradation of the metal complexes in four weeks. Thus, the complexes (**11** and **12**) demonstrated no leakage of metal ions and showed sufficient hydrolytic stability for them to act as potential catalysts in a relatively long time period, for example, in the RNase activity experiments carried out in this study.

2.4 | RNase Activity

The catalytic centers of natural nucleases usually contain one or two metal ions, which facilitate either hydrolytic or oxidative cleavage of nucleic acids. In the hydrolytic pathway, the metal ions contribute to the cleavage by a) acting as Lewis acids, thereby activating the phosphoryl group toward nucleophilic attack; b) decreasing the pK_a of the leaving group, thus enhancing the leaving group ability; c) deprotonating hydrating water molecules or other hydroxyl groups present, which increases the proportion of anionic nucleophiles; or d) holding the nucleophile and the substrate close to each other, therefore partially overcoming the electrostatic repulsion [48]. Metal-promoted cleavage of RNA is a combination of modes (a) and (c), where the metal ion assists the proton transfer from the attacking 2'-OH nucleophile to the leaving 5'-OH nucleophile. In the oxidative pathway, electron transfer from the metal to molecular oxygen or peroxide creates reactive oxygen species (ROS), which abstracts a hydrogen from the ribose or deoxyribose ring [59]. Subsequently, spontaneous cleavage of C–C and C–O bonds leads to strand scission. The metal complexes mimic, for example, nature's glycopeptoid bleomycin, a cancer drug, where the peptoid moiety is responsible for oxidative cleavage of DNA and RNA, and the saccharide moiety accounts for cellular uptake. Some other salen complexes have previously shown good ability to cleave RNA and DNA [60, 61].

The catalytic phosphodiester cleavage activity of the metal complexes (**11** and **12**) was studied using a biologically relevant sequence of HER2 RNA (5'-6FAM-GUG AGC ACC AUG GAG-3'). The oligonucleotide was labelled with fluorescein, and the degradation was analyzed by denaturing polyacrylamide gel electrophoresis (PAGE) to obtain $t_{1/2}$ values of the RNA's decay (Figure 3A). The cleavage was followed at 35°C and pH 7.5, and aliquots were withdrawn from the reaction solution at suitable time intervals. A fluorescein labelled 2'-OMe oligonucleotide (5'-6FAM-AAA AAA AAA AAA AAA AAA AAA-3') was used as an internal standard. All reactions were carried out in HEPES buffer (0.10 M, $I = 0.10$ M) in excess of the cleaving agent (50 μM **11**/**12** ($c_{eff} = 200$ μM), 50 μM

target-ON, 25 μM std-ON). The disappearance of the starting material followed first-order kinetics, exemplified by Figure 3b,c. For reference, we also followed the potential RNA cleavage with compounds **9** and **8**, as well as without any catalyst. The amounts of **9** (1 eq relative to **11**/**12**) and **8** (8 eq relative to **11**/**12**) were matched to the reaction conditions with **11** and **12**, or the catalyst was replaced with water. The reactions were also performed with only the metal precursors (i.e., no ligands) to see if the activity was in fact due to the whole complexes. The amount of metal precursors $Zn(OAc)_2$ and $Cu(OAc)_2$ (4 eq relative to **11**/**12**) was also matched to the reaction conditions with **11** and **12**. The metal complexes **11** and **12** exhibit RNase activity with half-lives of 146 h and 362 h, respectively (Table 1). The Zn^{2+} complex (**11**) proved to be a more active but modest catalyst for the HER2 RNA cleavage in comparison with artificial Zn^{2+} ion-based catalysts in general [62]. Compounds **8** and **9** induce negligible cleavage of the

target RNA. The metal precursors exhibit different, albeit faster, reaction rates than the respective metal complexes. Considering the hydrolytic stability of the complexes (**11** and **12**) and the kinetics of the RNA degradation, the catalytic activity, although modest, can be accounted for by the complexes.

3 | Conclusion

COSS-metallosalen-mannose complexes **11** and **12** were synthesized, and their identity was verified by NMR and mass spectrometry. The hydrolytic stability of these compounds was proven by NMR studies. In addition, crystal structures of model zinc and copper complexes (**13** and **14**) with the same tetranuclear core moiety were synthesized and crystallized to demonstrate the likely D_{4h} and S_4 symmetries of the respective mannose analogues (**11** and **12**). While the crystal structure of **13** has previously been published [37], the structure of the S_4 symmetric Cu^{2+} complex **14** was described for the first time. The potential variable D_{4h}/S_4 geometries of the COSS-metallosalen-mannose complexes (**11** and **12**) expectedly affect the orientation of the sugar moieties and the availability of the metal centers in potential catalytic cavities on the COSS core. Ribonuclease activity of **11** and **12** was studied using a biologically relevant RNA model as a target (HER2 RNA responsible for the expression of human epidermal growth factor receptor in many breast cancer types). The zinc(II) complex (**11**) showed higher activity than the copper(II) complex (**12**), but the activity remained modest compared to Zn-based artificial nucleases in general. Both zinc and copper are good Lewis acids, but the coordination chemistry of metallosalens might not be optimal for hydrolytic cleavage, as the metal ions are not as available to react with other surrounding hydroxyl groups. Modifying the ligand, for example, using hydroxysalens, might improve the catalytic activity [63].

Alternatively, a different target sequence for these complexes, or other metal ions for the cleavage of HER2, might show better activity, as certain sequences might be more prone to cleavage by certain complexes [60]. Metallosalens are redox active, so an oxidative cleavage pathway is more preferable for them than a hydrolytic one [61, 64]. However, whereas the 2'-OH group makes RNA more labile toward hydrolytic degradation, it stabilizes the sugar moiety in RNA against ROS [65]. ROS toward RNA may lead to base damage rather than strand cleavage. DNA is more susceptible to oxidative cleavage. There are plenty of examples where metallosalens have shown good DNase activity, but examples with good RNase activity are sparse [60, 61, 63]. As our interest lies in cleaving RNA (the HER2 model), cleavage of DNA was not explored. Since the cleavage activity was not at a desired level, no cell uptake studies were performed. Regardless, the good hydrolytic stability of these well-organized complexes and their efficient, good-yielding assembly on the COSS core can be utilized for the synthesis of other glyco or biomolecule analogues, possibly with more potent catalytic activity and RNA/cell receptor-binding properties.

TABLE 1 | First-order rate constants and half-lives of HER2 cleavage in HEPES buffer (0.10 M, $I = 0.10$ M) at 35°C and pH 7.5.

Catalyst	k /10^{-8} (s^{-1})	$t_{1/2}$ (h)
11	132 ± 1.41	146 ± 1.56
12	53.2 ± 0.60	362 ± 4.07
9	~ 6.55	~ 3000
8	stable	stable
No catalyst	stable	stable
$Zn(OAc)_2$	237 ± 3.38	81.0 ± 1.15
$Cu(OAc)_2$	56.3 ± 0.78	342 ± 4.69

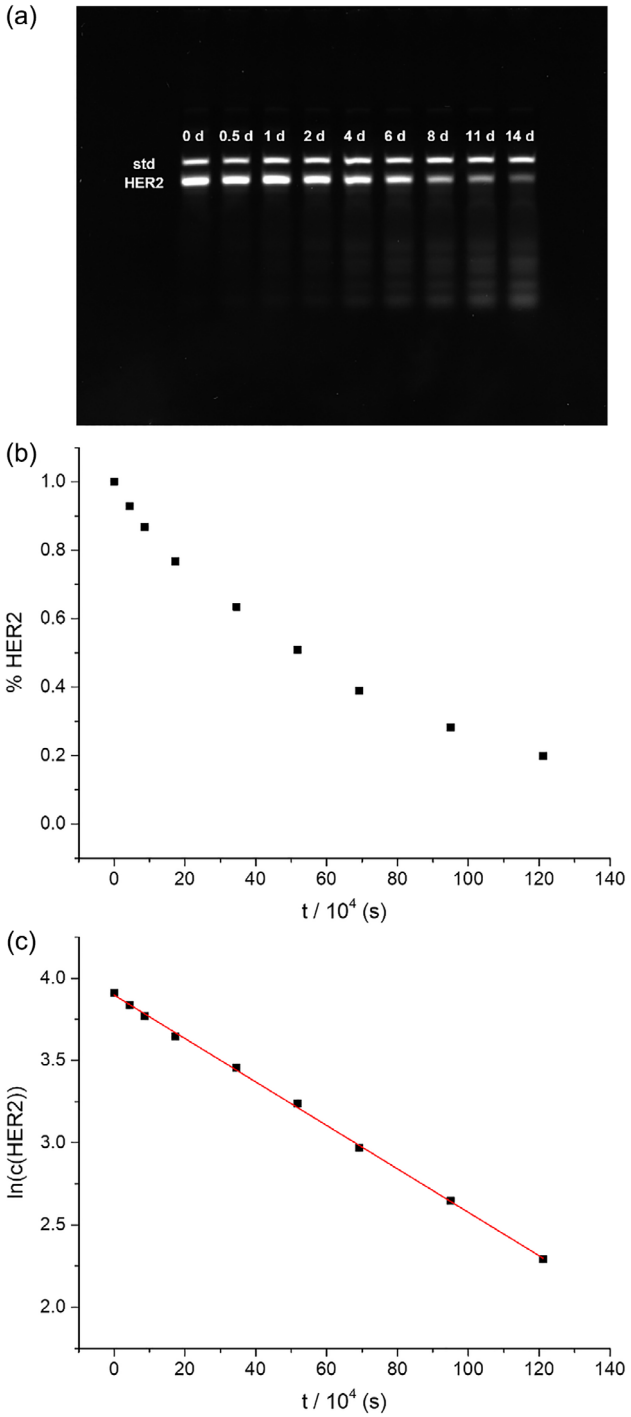

FIGURE 3 | Cleavage of HER2 by **11** in HEPES buffer (0.10 M, $I =$ 0.10 M) at 35°C and pH 7.5.

4 | Experimental Section

4.1 | General Methods and Materials

Oligonucleotides were synthesized by a conventional phosphoramidite strategy on a solid support using commercial phosphoramidite blocks. Deprotection and cleavage were performed with a 1:1 (*v/v*) mixture of 25% (*w/w*) aq ammonia and 40% (*w/w*) aq methylamine, and the crude oligonucleotides were purified by RP-HPLC using Phenomenex Clarity Oligo-RP (5 µm, 250 x 10 mm) semipreparative column. The yields of oligonucleotides were determined according to their UV absorbance at 260 nm. The mass spectra were recorded using a Waters Acquity UPLC-DAD RDa MS electrospray ionization time-of-flight (ESI-TOF) spectrometer. The ^{1}H, ^{13}C, and ^{29}Si NMR spectra were recorded on a Bruker Avance-III 500 MHz instrument equipped with a Prodigy BBO CryoProbe. Characterizations were made with additional information from DEPT-135, DQF-COSY, multiplicity edited HSQC, and HMBC experiments. The reported ^{1}H and ^{13}C NMR signals are referenced to the residual solvent signals [66], and the reported ^{29}Si signals are referenced to TMS (δ_{Si} = 0.00 ppm) added to the samples.

4.2 | Synthesis of 5-*tert*-butylsalicylaldehyde (2)

The reaction was performed according to a procedure from the literature [51].

4.3 | Synthesis of 3-bromomethyl-5-*tert*-butylsalicylaldehyde (3)

The reaction was performed according to a procedure from the literature [52].

4.4 | Synthesis of 3-azidomethyl-5-*tert*-butylsalicylaldehyde (4)

The reaction was performed according to a procedure from the literature [53].

4.5 | Synthesis of 2,3,4,6-tetra-*O*-acetyl-1-*O*-(3-butynyl)mannopyranoside (6)

The reaction was performed according to a procedure from the literature [54].

4.6 | Synthesis of tetraacetylated salicylaldehyde-mannose (7)

3-azidomethyl-5-*tert*-butylsalicylaldehyde (**4**, 0.1700 g, 1 eq), 2,3,4,6-tetra-*O*-acetyl-1-*O*-(3-butynyl)mannopyranoside (**6**, 0.2931 g, 1 eq), $CuSO_4$ (0.0117 g, 0.1 eq), and sodium ascorbate (0.0435 g, 0.3 eq) were dissolved in a 50:50 (*v/v*) mixture of MeCN and water (10 mL). The reaction was stirred at room temperature and followed by TLC (hexane/EtOAc 60:40 (*v/v*)) until no starting materials were visible. $CuSO_4$ (0.1 eq) and sodium ascorbate (0.3 eq) were added to the reaction mixture every one hour, as the product was noticed to coordinate copper a little bit. The reaction mixture was evaporated to dryness after 7 h. DCM and water were added to the evaporation residue, and the layers were separated. The aqueous layer was extracted with DCM (1×), and the combined organic layers were washed with saturated aqueous $NaHCO_3$ (2×), brine (2×), and water (2×). The organic layer was dried with Na_2SO_4 and evaporated *in vacuo* after filtration. The crude product was purified by silica gel column chromatography (DCM/MeOH 97:3 (*v/v*)), affording the product **7** as a white solid (0.33 g, 72%). ^{1}H NMR (500 MHz, $CDCl_3$, 25°C): δ = 11.26 (s, 1H), 9.89 (s, 1H), 7.62 (d, J = 2.5 Hz, 1H), 7.61 (s, 1H), 7.54 (d, J = 2.5 Hz, 1H), 5.56 (s, 2H), 5.24–5.32 (m, 2H), 5.20 (dd, J = 3.1, 1.7 Hz, 1H), 4.81 (d, J = 1.7 Hz, 1H), 4.25 (dd, J = 12.3, 5.2 Hz, 1H), 4.07 (dd, J = 12.3, 2.3 Hz, 1H), 3.97 (dt, J = 9.5, 6.6 Hz, 1H), 3.87 (ddd, J = 9.4, 5.2, 2.3 Hz, 1H), 3.70 (dt, J = 9.5, 6.6 Hz, 1H), 3.01 (dd, J = 6.6, 6.6 Hz, 2H), 2.14 (s, 3H), 2.07 (s, 3H), 2.05 (s, 3H), 2.01 (s, 3H), 1.30 ppm (s, 9H); ^{13}C{^{1}H} NMR (126 MHz, $CDCl_3$, 25°C): δ = 196.8, 170.8, 170.2, 170.1, 169.8, 157.3, 144.5, 143.4, 135.6, 131.0, 123.1, 122.8, 120.4, 97.7, 69.7, 69.2, 68.8, 67.3, 66.2, 62.5, 48.3, 34.3, 31.3, 26.4, 21.0, 20.9, 20.8 ppm; HRMS (ESI): *m/z* calcd for $C_{30}H_{39}N_3O_{12}$+H^+: 634.2607 [M+H]$^+$, found: 634.2593.

4.7 | Synthesis of salicylaldehyde-mannose (8)

Starting material **7** (0.1914 g, 1 eq) and K_2CO_3 (0.2505 g, 6 eq) were dissolved in MeOH (15 mL), and the reaction mixture was stirred overnight at room temperature. TLC analysis (EtOAc) indicated no starting material left after 24 h, so the reaction mixture was evaporated to dryness. The crude product was purified by silica gel column chromatography (EtOAc/MeOH 80:20 (*v/v*)), affording the product **8** as a light-yellow solid (0.10 g, 72%). ^{1}H NMR (500 MHz, CD_3OD, 25°C): δ = 9.93 (s, 1H), 7.83 (s, 1H), 7.75 (d, J = 2.5 Hz, 1H), 7.65 (d, J = 2.5 Hz, 1H), 5.60 (s, 2H), 4.76 (d, 1.7 Hz, 1H), 3.95 (dt, J = 9.7, 6.7 Hz, 1H), 3.79 (dd, J = 11.8, 2.3 Hz, 1H), 3.76 (dd, J = 3.1, 1.7 Hz, 1H), 3.57–3.71 (m, 4H), 3.40 (ddd, J = 9.3, 5.8, 2.3 Hz, 1H), 2.97 (dd, J = 6.7, 6.7 Hz, 2H), 1.32 ppm (s, 9H); ^{13}C{^{1}H} NMR (126 MHz, CD_3OD, 25°C): δ = 198.8, 158.0, 146.2, 144.4, 136.1, 132.3, 124.4, 124.2, 121.8, 101.6, 74.7, 72.5, 72.0, 68.5, 67.4, 62.8, 49.2, 35.1, 31.6, 27.0 ppm; HRMS (ESI) *m/z* calcd for $C_{22}H_{31}N_3O_8$+H^+: 466.2184 [M+H]$^+$, found: 466.2170.

4.8 | Synthesis of aminopropyl-COSS (9)

The synthesis process was modified from a procedure from the literature [55]. A solution of concentrated aqueous HCl (10 mL) and MeOH (110 mL) was heated to 60°C, and 3-aminopropyltriethoxysilane (**9**, 4.680 mL) was added dropwise to the reaction mixture. After addition, the reaction mixture was further heated to 90°C and stirred overnight. The solution was cooled to room temperature, and THF (220 mL) was added to precipitate the crude product. The precipitate was isolated by suction filtration and washed with THF. The crude product was recrystallized from MeOH and washed with Et_2O, affording the product **10** as a white solid (0.39 g, 13%). ^{1}H NMR (500 MHz, DMSO-*d6*, 25°C): δ = 8.24 (br, 24H), 2.79 (t, J = 7.6 Hz, 16H),

1.74 (m, 16H), 0.74 ppm (t, J = 8.0 Hz, 16H); $^{13}C\{^1H\}$ NMR (126 MHz, DMSO-*d6*, 25°C): δ = 41.0, 20.6, 8.4 ppm; $^{29}Si\{^1H\}$ NMR (99 MHz, DMSO-*d6*, 25°C): δ = −66.4 ppm; HRMS (ESI) *m/z* calcd for $C_{24}H_{64}N_8O_{12}Si_8+H^+$: 881.2871 $[M+H]^+$, found: 881.2874.

4.9 | Synthesis of COSS-salen-mannose (10)

Aminopropyl-COSS (**9**, 0.0150 g, 1 eq) and salicylaldehyde-mannose (**8**, 0.0595 g, 10 eq) were dissolved in anhydrous MeOH (5 mL), and triethylamine (42.7 µL, 24 eq) was added. The reaction mixture was stirred overnight at room temperature and then evaporated to dryness. The crude product (as a dry solid) was washed multiple times with CH_3Cl (to remove triethylamine chloride) and EtOAc (to remove the excess starting material **8**). The product was dissolved in MeOH, and evaporation to dryness afforded the product **10** as a yellow solid (0.056 g, 99%). ^1H NMR (500 MHz, CD_3OD, 25°C): δ = 8.33 (s, 8H), 7.73 (s, 8H), 7.32 (d, J = 2.4 Hz, 8H), 7.22 (d, J = 2.4 Hz, 8H), 5.44 (s, 16H), 4.73 (d, J = 1.6 Hz, 8H), 3.88 (dt, J = 9.7, 6.7 Hz, 8H), 3.78 (dd, J = 11.8, 2.4 Hz, 8H), 3.75 (dd, J = 3.2, 1.6 Hz, 8H), 3.57–3.70 (m, 32H), 3.53 (t, J = 6.3 Hz, 16H), 3.39 (ddd, J = 9.5, 5.7, 2.4 Hz, 8H), 2.87 (dd, J = 6.7, 6.7 Hz, 16H), 1.81 (m, 16H), 1.19 (s, 72H), 0.79 ppm (t, J = 7.8 Hz, 16H); $^{13}C\{^1H\}$ NMR (126 MHz, CD_3OD, 25°C): δ = 167.3, 162.0, 145.9, 141.3, 132.7, 130.3, 124.5, 124.3, 118.7, 101.5, 74.7, 72.6, 72.1, 68.6, 67.4, 62.9, 60.0, 50.1, 34.8, 31.8, 27.0, 25.5, 10.0 ppm; $^{29}Si\{^1H\}$ NMR (99 MHz, CD_3OD, 25°C): δ = −66.2 ppm. HRMS (ESI) *m/z* calcd for $C_{200}H_{296}N_{32}O_{68}Si_8+2H^{2+}$: 2229.9494 $[M+2H]^{2+}$, found: 2229.9409; *m/z* calcd for $C_{200}H_{296}N_{32}O_{68}Si_8+3H^{3+}$: 1486.9687 $[M+3H]^{3+}$, found: 1486.9664; *m/z* calcd for $C_{200}H_{296}N_{32}O_{68}Si_8+4H^{4+}$ 1115.4783 $[M+4H]^{4+}$, found: 1115.4745.

4.10 | Synthesis of COSS-salen-mannose-$Zn^{2+}{}_4$ (11)

Starting material **10** (5.1 mg, 1 eq) was dissolved in anhydrous MeOH (2.733 mL). $Zn(OAc)_2 \cdot 2H_2O$ in anhydrous MeOH (0.0364 M, 0.125 mL, 4 eq) was added, and the reaction mixture was stirred at room temperature for 2 h. The solution was then divided into 150 µL (60 nmol) aliquots, which were lyophilized. HRMS (ESI) *m/z* (most abundant) calcd for $C_{200}H_{288}N_{32}O_{68}Si_8Zn_4+2Na^{2+}$: 2380.2596 $[M+2Na]^{2+}$, found: 2380.2493.

4.11 | Synthesis of COSS-salen-mannose-$Cu^{2+}{}_4$ (12)

Starting material **10** (4.4 mg, 1 eq) was dissolved in anhydrous MeOH (2.255 mL). $Cu(OAc)_2$ in anhydrous MeOH (0.0187 M, 0.211 mL, 4 eq) was added, and the reaction mixture was stirred at room temperature for 2 h. The solution was then divided into 150 µl (60 nmol) aliquots, which were lyophilized. HRMS (ESI) *m/z* (most abundant) calcd for $C_{200}H_{288}N_{32}O_{68}Si_8Cu_4+3H^{3+}$: 1570.1883 $[M+3H]^{3+}$, found: 1570.1900; *m/z* (most abundant) calcd for $C_{200}H_{288}N_{32}O_{68}Si_8Cu_4+4H^{4+}$: 1177.8930 $[M+4H]^{4+}$, found: 1177.8980.

4.12 | Synthesis of COSS-di-*tert*-butylsalicylaldehyde (15)

Aminopropyl-COSS (**9**, 0.20 g, 1 eq) was dissolved in EtOH (6 mL), and triethylamine (106 µL, 8 eq) and 3,5-di-*tert*-butyl-salicylaldehyde (0.50 g, 22 eq) were added. The reaction mixture was stirred at room temperature overnight, after which it was evaporated to dryness. The crude product was dissolved in DCM and washed with water. The organic layer was dried with Mg_2SO_4 and then evaporated to dryness after filtration. The evaporation residue was washed multiple times with MeOH to remove the excess 3,5-di-*tert*-butyl-salicylaldehyde. The product was dissolved in DCM, and evaporation to dryness afforded the product as a yellow solid (0.132 g, 53%). ^1H NMR (500 MHz, $CDCl_3$, 25°C): δ = 13.96 (s, 8H), 8.33 (s, 8H), 7.35 (d, J = 2.4 Hz, 8H), 7.06 (d, J = 2.4 Hz, 8H), 3.55 (t, J = 6.6 Hz, 16H), 1.81 (m, 16H), 1.44 (s, 72H), 1.29 (s, 72H), 0.72 ppm (t, J = 8.4 Hz, 16H); $^{13}C\{^1H\}$ NMR (126 MHz, $CDCl_3$, 25°C): δ = 166.0, 158.4, 139.9, 136.7, 126.8, 118.0, 62.0, 35.2, 34.2, 31.7, 29.6, 24.6, 9.7 ppm; $^{29}Si\{^1H\}$ NMR (99 MHz, $CDCl_3$, 25°C): δ = −66.74 ppm.

4.13 | Synthesis of COSS-di-*tert*-butylsalicylaldehyde-$Zn^{2+}{}_4$ (13)

Starting material **15** (5.2 mg, 1 eq) was dissolved in a 1:1 (*v/v*) mixture of CH_3Cl and MeOH (1 mL). $Zn(OAc)_2 \cdot 2H_2O$ in a 1:1 (*v/v*) mixture of CH_3Cl and MeOH (0.01 M, 0.8 mL, 4 eq) was added, and the solution was left crystallizing at room temperature.

4.14 | Synthesis of COSS-di-*tert*-butylsalicylaldehyde-$Cu^{2+}{}_4$ (14)

Starting material **15** (7.8 mg, 1 eq) was dissolved in CH_3Cl (1.5 mL). $Cu(OAc)_2 \cdot H_2O$ in MeOH (0.01 M, 0.96 mL, 4 eq) was added, and the solution was left crystallizing at room temperature.

4.15 | Kinetic Experiments

The reactions were carried out in Eppendorf tubes and heated at 35°C with a dry heat block. 20 µL HEPES buffer (0.40 M in H_2O, pH 7.5, ionic strength adjusted to 0.40 M with NaCl), 20 µL internal standard oligonucleotide (100 µM in H_2O), 20 µL target oligonucleotide (200 µM in H_2O), and 20 µL catalyst **11**/**12** (200 µM in H_2O/DMSO 3:1 (*v/v*)) were added to an Eppendorf tube. Consequently, the total reaction volume was 80 µL (c(HEPES) = 0.10 M), I(HEPES) = 0.1 M, c(std-ON) = 25 µM, c(target-ON) = 50 µM, c(cat.) = 50 µM) with a pH of 7.5. In the reference reactions, 20 µL **9** (200 µM), 20 µL **8** (1.6 mM), 20 µL H_2O, 20 µL $Zn(OAc)_2 \cdot 2H_2O$ (800 µM), or 20 µL $Cu(OAc)_2$ (800 µM) was added instead of the catalyst **11**/**12** to match the reaction conditions. 4 µL aliquots were withdrawn at suitable time intervals and cooled immediately on an ice-water bath. The aliquots were diluted 10-fold with H_2O, and a 4 µL sample from the dilution was mixed with 4 µL Novex TBE-Urea 2× sample buffer. The samples were frozen with liquid N_2 and kept

in a freezer until denaturing polyacrylamide gel electrophoresis (PAGE) was performed to analyze the cleavage of HER2. 6 μL of the samples were applied to gel wells. The gel used was a TBE-Urea gel (15% acrylamide, 1×TBE, 7 M urea) fixed into a vertical electrophoresis chamber, which was filled with the running buffer (90 mM Tris, 90 mM borate, 2 mM EDTA, pH 8.3). The gels were run at 200 V and 45 mA for 45 min, and they were imaged by the fluorescence labels in the standard oligonucleotide and the target oligonucleotide. The bands on the gels were quantified by processing the images into 2D density profiles and integrating them using ImageJ software. The values obtained for HER2 were corrected by dividing them by the values obtained for the standard, and then normalized to the starting point. First-order rate constants were calculated for the disappearance of the target oligonucleotide by applying the integrated first-order rate law to the diminution of the signal from HER2.

Acknowledgments

Financial support from the Doctoral Programme in Exact Sciences (EXACTUS), University of Turku, and from the Turku University Foundation is gratefully acknowledged. We also wish to gratefully acknowledge the Turku Bioscience Protein Structure and Chemistry Core Facility, a member of Biocenter Finland and FINStruct, for their expertise and for providing access to the single-crystal X-ray diffraction instrument.

Open access publishing facilitated by Turun yliopisto, as part of the Wiley - FinELib agreement.

Conflicts of Interest

The authors declare no conflict of interest.

Data Availability Statement

The data that support the findings of this study are available from the corresponding author upon reasonable request.

References

1. C. Domingues, A. Santos, C. Alvarez-Lorenzo, et al., "Where Is Nano Today and Where Is It Headed? A Review of Nanomedicine and the Dilemma of Nanotoxicology," *ACS Nano* 16, no. 7 (2022): 9994.

2. P. D. Lickiss and F. Rataboul, "Chapter 1: Fully Condensed Polyhedral Oligosilsesquioxanes (POSS): From Synthesis to Application," (Eds.: A. F. Hill, M. J. Fink) in *Advances in Organometallic Chemistry* (Elsevier Inc., 2008): 1–116, ISBN 978-0-12-374465-4.

3. D. B. Cordes, P. D. Lickiss, and F. Rataboul, "Recent Developments in the Chemistry of Cubic Polyhedral Oligosilsesquioxanes," *Chemical Reviews* 110, no. 4 (2010): 2081–2173, https://doi.org/10.1021/cr900201r.

4. G. Kickelbick, "Silsesquioxanes," in *Functional Molecular Silicon Compounds I. Structure and Bonding* (Ed.: D. Scheschkewitz) (Springer, 2013): 1–28, ISBN 978-3-319-03620-5.

5. A. Kannan, C. Muthuraj, A. Mayavan, and S. Gandhi, "Multifaceted Applications of Polyhedral Oligomeric Silsesquioxane and Their Composites," *Materials Today Chemistry* 30 (2023): 101568, https://doi.org/10.1016/j.mtchem.2023.101568.

6. Eds. S. Kalia, K. Pielichowski, *Polymer/POSS Nanocomposites and Hybrid Materials—Preparation, Properties, Applications*, (Springer International Publishing, 2018). ISBN 978-3-030-02327-0.

7. F. Dong, L. Lu, and C.-S. Ha, "Silsesquioxane-Containing Hybrid Nanomaterials: Fascinating Platforms for Advanced Applications," *Macromolecular Chemistry and Physics* 220, no. 3 (2019): 1800324, https://doi.org/10.1002/macp.201800324.

8. J. Henig, É. Tóth, J. Engelmann, S. Gottschalk, and H. A. Mayer, "Macrocyclic Gd3+ Chelates Attached to a Silsesquioxane Core as Potential Magnetic Resonance Imaging Contrast Agents: Synthesis, Physicochemical Characterization, and Stability Studies," *Inorganic Chemistry* 49, no. 13 (2010): 6124–6138, https://doi.org/10.1021/ic1007395.

9. W. H. Siddiqui and R. G. York, "Quaternary Silsesquioxane: a Developmental Toxicity Study in Rats," *Fundamental and Applied Toxicology* 21, no. 1 (1993): 66–70, https://doi.org/10.1006/faat.1993.1073.

10. S. Fabritz, S. Hörner, O. Avrutina, and H. Kolmar, "Bioconjugation on Cube-Octameric Silsesquioxanes," *Organic & Biomolecular Chemistry* 11, no. 14 (2013): 2224, https://doi.org/10.1039/c2ob26807h.

11. P. H. Ehrlich, "The Effect of Multivalency on the Specificity of Protein and Cell Interactions," *Journal of Theoretical Biology* 81, no. 1 (1979): 123–127, https://doi.org/10.1016/0022-5193(79)90085-7.

12. M. Mammen, S.-K. Choi, and G. M. Whitesides, "Polyvalent Interactions in Biological Systems: Implications for Design and Use of Multivalent Ligands and Inhibitors," *Angewandte Chemie International Edition* 37, no. 20 (1998): 2754–2794, https://doi.org/10.1002/(SICI)1521-3773(19981102)37:20%3c2754::AID-ANIE2754%3e3.0.CO;2-3.

13. R. T. Lee and Y. C. Lee, "Affinity Enhancement by Multivalent Lectin-Carbohydrate Interaction," *Glycoconj J* 17, no. 7–9 (2000): 543.

14. A. Arsiwala, A. Castro, S. Frey, M. Stathos, and R. S. Kane, "Designing Multivalent Ligands to Control Biological Interactions: From Vaccines and Cellular Effectors to Targeted Drug Delivery," *Chemistry—An Asian Journal* 14, no. 2 (2019): 244–255, https://doi.org/10.1002/asia.201801677.

15. T. A. Wynn, A. Chawla, and J. W. Pollard, "Macrophage Biology in Development, Homeostasis and Disease," *Nature* 496, no. 7446 (2013): 445–455, https://doi.org/10.1038/nature12034.

16. J. Jantsch, K. J. Binger, D. N. Müller, and J. Titze, "Macrophages in Homeostatic Immune Function," *Frontiers in Physiology* 5 (2014): 146, https://doi.org/10.3389/fphys.2014.00146.

17. D. M. Mosser, K. Hamidzadeh, and R. Goncalves, "Macrophages and the Maintenance of Homeostasis," *Cellular & Molecular Immunology* 18, no. 3 (2021): 579–587, https://doi.org/10.1038/s41423-020-00541-3.

18. M. A. Elhelu, "The Role of Macrophages in Immunology," *Journal of the National Medical Association* 75, no. 3 (1983): 314.

19. C. Bogdan, "Macrophages," in *Encyclopedia of Life Sciences* (John Wiley & Sons, Ltd., 2006), https://doi.org/10.1038/NPG.ELS.0004007. ISBN 978-0-470-01590-2.

20. G. Weiss and U. E. Schaible, "Macrophage Defense Mechanisms Against Intracellular Bacteria," *Immunological Reviews* 264, no. 1 (2015): 182–203, https://doi.org/10.1111/imr.12266.

21. C. Zhang, M. Yang, and A. C. Ericsson, "Function of Macrophages in Disease: Current Understanding on Molecular Mechanisms," *Frontiers in Immunology* 12: 620510, https://doi.org/10.3389/fimmu.2021.620510.

22. E. A. Ross, A. Devitt, and J. R. Johnson, "Macrophages: the Good, the Bad, and the Gluttony," *Frontiers in Immunology* 12: 708186, https://doi.org/10.3389/fimmu.2021.708186.

23. T. Hagemann, J. Wilson, F. Burke, et al., "Ovarian Cancer Cells Polarize Macrophages Toward a Tumor-Associated Phenotype," *The Journal of Immunology* 176, no. 8 (2006): 5023–5032, https://doi.org/10.4049/jimmunol.176.8.5023.

24. P. Allavena, M. Chieppa, G. Bianchi, et al., "Engagement of the Mannose Receptor by Tumoral Mucins Activates an Immune Suppressive Phenotype in Human Tumor-Associated Macrophages," *Journal of Immunology Research* 2010, no. 1 (2010): 547179, https://doi.org/10.1155/2010/547179.

25. A. K. Azad, M. V. S. Rajaram, W. L. Metz, et al., "γ-Tilmanocept, a New Radiopharmaceutical Tracer for Cancer Sentinel Lymph Nodes, Binds to the Mannose Receptor (CD206)," *The Journal of Immunology* 195, no. 5 (2015): 2019–2029, https://doi.org/10.4049/jimmunol.1402005.

26. J. W. Pollard, "Tumour-Educated Macrophages Promote Tumour Progression and Metastasis," *Nature Reviews Cancer* 4, no. 1 (2004): 71–78, https://doi.org/10.1038/nrc1256.

27. C. E. Lewis and J. W. Pollard, "Distinct Role of Macrophages in Different Tumor Microenvironments," *Cancer Research* 66, no. 2 (2006): 605–612, https://doi.org/10.1158/0008-5472.CAN-05-4005.

28. P. Allavena, A. Sica, G. Solinas, C. Porta, and A. Mantovani, "The Inflammatory Micro-Environment in Tumor Progression: The Role of Tumor-Associated Macrophages," *Critical Reviews in Oncology/Hematology* 66, no. 1 (2008): 1–9, https://doi.org/10.1016/j.critrevonc.2007.07.004.

29. B.-Z. Qian and J. W. Pollard, "Macrophage Diversity Enhances Tumor Progression and Metastasis," *Cell* 141, no. 1 (2010): 39–51, https://doi.org/10.1016/j.cell.2010.03.014.

30. R. Noy and J. W. Pollard, "Tumor-Associated Macrophages: From Mechanisms to Therapy," *Immunity* 41, no. 1 (2014): 49.

31. C. B. Williams, E. S. Yeh, and A. C. Soloff, "Tumor-Associated Macrophages: Unwitting Accomplices in Breast Cancer Malignancy," *npj Breast Cancer* 2016, 2, no. 1: 1.

32. C. E. Lewis, A. S. Harney, and J. W. Pollard, "The Multifaceted Role of Perivascular Macrophages in Tumors," *Cancer Cell* 30, no. 1 (2016): 18–25, https://doi.org/10.1016/j.ccell.2016.05.017.

33. A. Mantovani, F. Marchesi, A. Malesci, L. Laghi, and P. Allavena, "Tumour-Associated Macrophages as Treatment Targets in Oncology," *Nature Reviews Clinical Oncology* 14, no. 7 (2017): 399–416, https://doi.org/10.1038/nrclinonc.2016.217.

34. P. Scrimin, M. A. Cardona, C. M. L. Prieto, and L. J. Prins, "Chapter 7: Multivalency as a Design Criterion in Catalyst Development," in *Multivalency* Eds.: J. Huskens, L. J. Prins, R. Haag, and B. J. Ravoo, (John Wiley & Sons, 2018): 153–176, https://doi.org/10.1002/9781119143505. ISBN 978-1-119-14350-5.

35. F. Mancin, L. J. Prins, P. Pengo, L. Pasquato, P. Tecilla, and P. Scrimin, "Hydrolytic Metallo-Nanozymes: From Micelles and Vesicles to Gold Nanoparticles," *Molecules (Basel, Switzerland)* 21, no. 8 (2016): 1014, https://doi.org/10.3390/molecules21081014.

36. K. Philippot and P. Serp, "Chapter 1: Concepts in Nanocatalysis," in *Nanomaterials in Catalysis* Eds.: P. Serp, (Wiley-VCH Verlag GmbH & Co. KGaA, 2013): 1–54, https://doi.org/10.1002/9783527656875. ISBN 978-3-527-65687-5.

37. M. Janeta, T. Lis, and S. Szafert, "Zinc Imine Polyhedral Oligomeric Silsesquioxane as a Quattro-Site Catalyst for the Synthesis of Cyclic Carbonates From Epoxides and Low-Pressure CO 2," *Chemistry—A European Journal* 26, no. 60 (2020): 13686–13697, https://doi.org/10.1002/chem.202002996.

38. R. Maity, B. S. Birenheide, F. Breher, and B. Sarkar, "Cooperative Effects in Multimetallic Complexes Applied in Catalysis," *Chemcatchem* 13, no. 10 (2021): 2337–2370, https://doi.org/10.1002/cctc.202001951.

39. A. Gualandi, F. Calogero, S. Potenti, and P. G. Cozzi, "Al(Salen) Metal Complexes in Stereoselective Catalysis," *Molecules (Basel, Switzerland)* 24, no. 9 (2019): 1716, https://doi.org/10.3390/molecules24091716.

40. E. Kabir, M. R. O. K. Noyon, and M. A. Hossain, "Synthesis, Biological and Medicinal Impacts of Metallodrugs: a Study," *Results in Chemistry* 5 (2023): 100935, https://doi.org/10.1016/j.rechem.2023.100935.

41. R. Paprocka, M. Wiese-Szadkowska, S. Janciauskiene, T. Kosmalski, M. Kulik, and A. Helmin-Basa, "Latest Developments in Metal Complexes as Anticancer Agents," *Coordination Chemistry Reviews* 452 (2022): 214307.

42. W. Yang, "Nucleases: Diversity of Structure, Function and Mechanism," *Quarterly Reviews of Biophysics* 44, no. 1 (2011): 1–93, https://doi.org/10.1017/S0033583510000181.

43. C. M. Dupureur, "Roles of Metal Ions in Nucleases," *Current Opinion in Chemical Biology* 12, no. 2 (2008): 250–255, https://doi.org/10.1016/j.cbpa.2008.01.012.

44. G. Palermo, A. Cavalli, M. L. Klein, M. Alfonso-Prieto, M. Dal Peraro, and M. De Vivo, "Catalytic Metal Ions and Enzymatic Processing of DNA and RNA," *Accounts of Chemical Research* 48, no. 2 (2015): 220–228, https://doi.org/10.1021/ar500314j.

45. F. Mancin, P. Scrimin, P. Tecilla, and U. Tonellato, "Artificial Metallonucleases," *Chemical Communications* no. 20 (2005): 2540–2548, https://doi.org/10.1039/b418164f.

46. F. Mancin, P. Scrimin, and P. Tecilla, "Progress in Artificial Metallonucleases," *Chemical Communications* 48, no. 45 (2012): 5545, https://doi.org/10.1039/c2cc30952a.

47. D. Desbouis, I. P. Troitsky, M. J. Belousoff, L. Spiccia, and B. Graham, "Copper(II), Zinc(II) and Nickel(II) Complexes as Nuclease Mimetics," *Coordination Chemistry Reviews* 256, no. 11–12 (2012): 897–937, https://doi.org/10.1016/j.ccr.2011.12.005.

48. M. Diez-Castellnou, A. Martinez, and F. Mancin, "Chapter 4: Phosphate Ester Hydrolysis: the Path From Mechanistic Investigation to the Realization of Artificial Enzymes," in *Advances in Physical Organic Chemistry* Eds.: I. H. Williams, N. H. Williams, (Academic Press, 2017): 129–186. ISBN 978-0-128-12094-1.

49. Z. Yu and J. A. Cowan, "Metal Complexes Promoting Catalytic Cleavage of Nucleic Acids — Biochemical Tools and Therapeutics," *Current Opinion in Chemical Biology* 43 (2018): 37–42, https://doi.org/10.1016/j.cbpa.2017.10.029.

50. M. D. Tomczyk, N. Kuźnik, and K. Walczak, "Cyclen-Based Artificial Nucleases: Three Decades of Development (1989–2022). Part a—Hydrolysis of Phosphate Esters," *Coordination Chemistry Reviews* 481 (2023): 215047, https://doi.org/10.1016/j.ccr.2023.215047.

51. S. Bhatt and S. K. Nayak, "Reductive Deoxygenation of Ortho-Hydroxyaromatic Aldehydes to 1,2-Bis(Hydroxyaryl)Ethanes: Application to the Synthesis of Ethylene Bridged Calixarene-Analogous Metacyclophanes," *Tetrahedron Letters* 50, no. 42 (2009): 5823–5826, https://doi.org/10.1016/j.tetlet.2009.07.156.

52. Q. Wang, C. Wilson, A. J. Blake, S. R. Collinson, P. A. Tasker, and M. Schröder, "The One-Pot Halomethylation of 5-Substituted Salicylaldehydes as Convenient Precursors for the Preparation of Heteroditopic Ligands for the Binding of Metal Salts," *Tetrahedron Letters* 47, no. 50 (2006): 8983–8987, https://doi.org/10.1016/j.tetlet.2006.09.149.

53. J. Schmid, W. Frey, and R. Peters, "Polynuclear Enantiopure Salen–Mesoionic Carbene Hybrid Complexes," *Organometallics* 36, no. 21 (2017): 4313–4324, https://doi.org/10.1021/acs.organomet.7b00729.

54. A. Kiviniemi, P. Virta, and H. Lönnberg, "Utilization of Intrachain 4′-C-Azidomethylthymidine for Preparation of Oligodeoxyribonucleotide Conjugates by Click Chemistry in Solution and on a Solid Support," *Bioconjugate Chemistry* 19, no. 8 (2008): 1726–1734, https://doi.org/10.1021/bc800221p.

55. Y. J. Pu, H. Yuan, M. Yang, B. He, and Z. W. Gu, "Synthesis of Peptide Dendrimers With Polyhedral Oligomeric Silsesquioxane Cores via Click Chemistry," *Chinese Chemical Letters* 24, no. 10 (2013): 917–920, https://doi.org/10.1016/j.cclet.2013.06.015.

56. C. R. Groom, I. J. Bruno, M. P. Lightfoot, and S. C. Ward, "The Cambridge Structural Database," *Acta Cryst* B72, no. 2 (2016): 171.

57. L. Yang, D. R. Powell, and R. P. Houser, "Structural Variation in Copper(I) Complexes With Pyridylmethylamide Ligands: Structural Analysis With a New Four-Coordinate Geometry Index, T4," *Dalton Transactions* no. 9 (2007): 955–964, https://doi.org/10.1039/B617136B.

58. A. Tzubery and E. Y. Tshuva, "Cytotoxicity and Hydrolysis of Trans -Ti(IV) Complexes of Salen Ligands: Structure–Activity Relationship Studies," *Inorganic Chemistry* 51, no. 3 (2012): 1796–1804, https://doi.org/10.1021/ic202092u.

59. Q. Jiang, N. Xiao, P. Shi, Y. Zhu, and Z. Guo, "Design of Artificial Metallonucleases With Oxidative Mechanism," *Coordination Chemistry Reviews* 251, no. 15–16 (2007): 1951–1972, https://doi.org/10.1016/j.ccr.2007.02.013.

60. A. M. Kaczmarek, P. W. A. Porebski, T. Mortier, F. Lynen, R. Van Deun, and K. Van Hecke, "Near-Infrared Luminescence and RNA Cleavage Ability of Lanthanide Schiff Base Complexes Derived From N,N′-Bis(3-Methoxysalicylidene)Ethylene-1,2-Diamine Ligands," *Journal of Inorganic Biochemistry* 163 (2016): 194–205, https://doi.org/10.1016/j.jinorgbio.2016.07.017.

61. A. Erxleben, "Transition Metal Salen Complexes in Bioinorganic and Medicinal Chemistry," *Inorganica Chimica Acta* 472 (2018): 40–57, https://doi.org/10.1016/j.ica.2017.06.060.

62. S. Mikkola, T. Lönnberg, and H. Lönnberg, "Phosphodiester Models for Cleavage of Nucleic Acids," *Beilstein Journal of Organic Chemistry* 14, no. 1 (2018): 803–837, https://doi.org/10.3762/bjoc.14.68.

63. C. Bailly, V. Guerniou, E. Lamour, J.-L. Bernier, F. Villain, and H. Vezin, "Site-Specific Cleavage of the HIV-1 TAR RNA by a Hydroxysalen–Copper(III) Complex," *Chembiochem* 4, no. 1 (2003): 112–114, https://doi.org/10.1002/cbic.200390003.

64. S. E. Rokita and C. J. Burrows, "Chapter 6: Salen–Metal Complexes," in *Small Molecule DNA and RNA Binders: From Synthesis to Nucleic Acid Complexes* Eds.: M. Demeunynck, C. Bailly, W. D. Wilson, (Wiley-VCH Verlag GmbH & Co. KGaA, 2002): 126–145.

65. H. H. Thorp, "The Importance of Being R: Greater Oxidative Stability of RNA Compared With DNA," *Chemistry & Biology* 7, no. 2 (2000): R33–R36, https://doi.org/10.1016/S1074-5521(00)00080-6..

66. G. R. Fulmer, A. J. M. Miller, N. H. Sherden, et al., "NMR Chemical Shifts of Trace Impurities: Common Laboratory Solvents, Organics, and Gases in Deuterated Solvents Relevant to the Organometallic Chemist," *Organometallics* 29, no. 9 (2010): 2176.

67. Agilent (2014), CrysAlisPro, Agilent Technologies Ltd, Yarnton, Oxfordshire, England.

68. G. M. Sheldrick, "SHELXT—Integrated Space-Group and Crystal-Structure Determination," *Acta Crystallographica* A71, no. 1 (2015): 3.

69. G. M. Sheldrick, "Crystal Structure Refinement With SHELXL," *Acta Crystallographica* C71, no. 1 (2015): 3.

70. O. V. Dolomanov, L. J. Bourhis, R. J. Gildea, J. A. K. Howard, and H. Puschmann, "OLEX2: A Complete Structure Solution, Refinement and Analysis Program," *Journal of Applied Crystallography* 42, no. 2 (2009): 339–341, https://doi.org/10.1107/S0021889808042726.

Supporting Information

Additional supporting information can be found online in the Supporting Information section.

The authors have cited additional references within the Supporting Information [67–70]. CCDC-2499417 contains the supplementary crystallographic data for this paper. These data can be obtained free of charge from The Cambridge Crystallographic Data Center via www.ccdc.cam.ac.uk/data_request/cif.

Supporting File: slct72615-sup-0001-SuppMat.pdf.